RESEARCH ARTICLES

CANCER THERAPY

Patient-derived models of acquired resistance can identify effective drug combinations for cancer

Adam S. Crystal,[1] Alice T. Shaw,[1] Lecia V. Sequist,[1] Luc Friboulet,[1] Matthew J. Niederst,[1] Elizabeth L. Lockerman,[1] Rosa L. Frias,[1] Justin F. Gainor,[1] Arnaud Amzallag,[1] Patricia Greninger,[1] Dana Lee,[1] Anuj Kalsy,[1] Maria Gomez-Caraballo,[1] Leila Elamine,[1] Emily Howe,[1] Wooyoung Hur,[3,4] Eugene Lifshits,[1] Hayley E. Robinson,[2] Ryohei Katayama,[1] Anthony C. Faber,[1] Mark M. Awad,[1] Sridhar Ramaswamy,[1] Mari Mino-Kenudson,[2] A. John Iafrate,[2] Cyril H. Benes,[1]* Jeffrey A. Engelman[1]*

Targeted cancer therapies have produced substantial clinical responses, but most tumors develop resistance to these drugs. Here, we describe a pharmacogenomic platform that facilitates rapid discovery of drug combinations that can overcome resistance. We established cell culture models derived from biopsy samples of lung cancer patients whose disease had progressed while on treatment with epidermal growth factor receptor (EGFR) or anaplastic lymphoma kinase (ALK) tyrosine kinase inhibitors and then subjected these cells to genetic analyses and a pharmacological screen. Multiple effective drug combinations were identified. For example, the combination of ALK and MAPK kinase (MEK) inhibitors was active in an *ALK*-positive resistant tumor that had developed a *MAP2K1* activating mutation, and the combination of EGFR and fibroblast growth factor receptor (FGFR) inhibitors was active in an *EGFR* mutant resistant cancer with a mutation in *FGFR3*. Combined ALK and SRC (pp60c-src) inhibition was effective in several ALK-driven patient-derived models, a result not predicted by genetic analysis alone. With further refinements, this strategy could help direct therapeutic choices for individual patients.

Genotype-based selection of patients for the application of targeted therapies has had a substantial impact on the treatment of cancers. Effective targeted therapies, such as tyrosine kinase inhibitors (TKIs), are widely used to treat patients harboring non–small cell lung cancers (NSCLCs) with activating mutations in *EGFR* (epidermal growth factor receptor) or *ALK* (anaplastic lymphoma kinase) translocations (*1*–*5*). However, acquired resistance to these inhibitors eventually develops through a variety of mechanisms, usually within 1 to 2 years [EGFR inhibitors are reviewed in (*6*) and ALK inhibitors in (*7*–*9*)]. In particular, secondary resistance mutations can develop in the oncogene preventing target inhibition by the corresponding TKI (e.g., EGFR T790M or ALK L1196M). Alternatively, resistant cells can develop a compensatory signaling pathway, or "bypass track," that reestablishes activation of key downstream proliferation and survival signals despite inhibition of the original oncogene [reviewed in (*10*)]. As more drugs are developed that effectively overcome secondary resistance mutations in the targeted genes, these bypass track mechanisms of resistance will likely continue to emerge in the clinical setting.

Current efforts to understand resistance often center on two different strategies. One approach is to model the development of resistance in vitro using sensitive cell line models that are exposed to a specific targeted therapy until resistance emerges. A second approach focuses on the genetic analyses of resistant biopsies to identify new genetic anomalies that could be driving resistance. However, both approaches have deficiencies. Although the in vitro–derived resistant cells are amenable to functional studies, it is unknown which models are clinically relevant, and they could never be used to inform treatment decisions for individual patients. Furthermore, there are few genetically appropriate cell lines in existence that could be used to develop such resistant models (e.g., there are less than 10 existing *EGFR* mutant and less than 5 *EML4-ALK* cell lines). Thus, these lines may model only a subset of potential resistance mechanisms. In contrast, studying the genetics of resistant biopsies has the advantage that the discovered genetic alterations actually occurred clinically. These studies can facilitate the development of hypotheses about what is causing resistance, and even speculation as to how one might treat individual patients. However, since the tissue is nonviable, such hypotheses cannot be directly tested on the resistant tumor cells. Furthermore, many resistant cancers do not harbor genetic abnormalities that clearly point to a treatment strategy. In this study, we describe a discovery platform that integrates the genetics of cancers with acquired resistance with pharmacologic interrogation of cell lines systematically developed from those same resistant patient tumors. This permits the discovery and evaluation of therapeutic strategies for clinically relevant mechanisms of resistance.

Establishment of resistant cell lines from clinical specimens

The ability to develop cell lines directly from patient specimens has been facilitated by recent technological advances, including methodologies developed by Schlegel and colleagues using irradiated feeder cells (*11*). As shown in table S1, NSCLC cell lines were developed with a ~50% success rate from patient samples (effusions and biopsies), including a 38% success rate from biopsy samples. Of note, the majority of the failures were associated with low cancer cellularity in the sample (see below). For many of these samples, cell viability was established on feeder cells and then transitioned off those cells before characterization and screening. As shown in table S2, the oncogenic mutation (*EGFR* or *ALK*) present in the patient tumor was reliably identified in the derived cell line.

To identify effective drug combinations in these patient-derived models of acquired resistance, we built upon previous work identifying bypass track mechanisms of acquired resistance (*10*). In this type of resistance, the original driver oncogene and a secondary bypass track redundantly maintain downstream signaling, such as the phosphatidylinositol 3-kinase (PI3K) and mitogen-activated protein kinase (MAPK) pathways, to promote cell survival and proliferation. These cancers are resistant to single-agent inhibition of the primary driver oncogene and are similarly resistant to single-agent inhibition of the acquired bypass track because, in either case, the untargeted pathway maintains downstream signaling. However, simultaneous inhibition of both pathways suppresses downstream signaling, resulting in growth arrest and cell death (fig. S1A) (*12*–*15*). Thus, drugs targeting relevant bypass tracks are effective when administered in combination with an inhibitor of the primary driver oncogene but relatively impotent when administered as single agents (fig. S1B). Based on this principle, to discover effective therapeutic strategies and gain insight into the underlying mechanisms of resistance, we performed a screen that combined the original TKI (targeting the driving oncogene) with each of the drugs in an established panel.

[1]Massachusetts General Hospital Cancer Center, Department of Medicine and Harvard Medical School, Boston, MA 02114, USA. [2]Massachusetts General Hospital Cancer Center, Department of Pathology and Harvard Medical School, Boston, MA 02114, USA. [3]Dana-Farber Cancer Institute, Department of Biological Chemistry and Molecular Pharmacology and Harvard Medical School, Boston, MA 02115, USA. [4]Chemical Kinomics Research Center, Korea Institute of Science and Technology, Seoul, 136-791, South Korea.
*Corresponding author. E-mail: jengelman@partners.org (J.A.E.); cbenes@partners.org (C.H.B.)

We assembled a panel of 76 targeted agents (table S3) directed against a range of key regulators of cell proliferation and survival, including growth factor and development signaling pathways, apoptosis regulators, transcription and protein folding machinery, and DNA damage sensors (table S4). This drug panel included inhibitors of previously identified bypass tracks, as well as several additional clinical targets. The potency of each drug was tested across a 10,000-fold range both in the presence and absence of a fixed concentration of the primary TKI (fig. S2A). Resultant changes in GI50 (the drug concentration necessary to obtain 50% less cells than in the untreated condition) and AUC (area under the dose-response curve) were determined after addition of the primary TKI.

To evaluate the potential of our strategy, we initially examined five previously established models of acquired resistance developed in vitro (i.e., by chronically exposing sensitive cells to TKI in vitro) with known resistance bypass tracks. In these models, the known mechanisms of resistance were identified by our approach with high specificity: For example, in a previously characterized *EGFR* mutant cell line with *MET* amplification (*12*), the MET inhibitors were the sole hits identified in the screen (fig. S2, B and C). In four tested cell lines [HCC827 GR6 (*13*), HN11 GR (*16*), SNU638 C1 (*17*), and H3122 PFR3 (*7*)], drugs that target known bypass tracks were among those producing the largest shifts in GI50 and AUC (fig. S3, A to D). In the fifth model [A431 GR (*16*)], the effect of insulin-like growth factor receptor 1 (IGFR1) inhibitors was less marked but recapitulated the previously observed combination effect (fig. S3E). Thus, in these previously investigated models, unbiased screening of a 76-drug panel successfully identified inhibitors of the known bypass tracks. We therefore applied the approach to 55 models of acquired resistance with unknown mechanisms of resistance. Twenty of these models were derived directly from patients who had progressed on either an ALK inhibitor (n = 9 models) or an EGFR inhibitor (n = 11 models). The remaining lines were derived in vitro (table S5). To compare the information yielded by genetic analysis to the pharmacologic interrogation, patient-derived models were also analyzed by next-generation sequencing to identify potential genetic causes of resistance (tables S6 and S7 and databases S1 and S2).

Effective drug combinations in patient-derived resistant NSCLC models

Each of the 55 models of acquired resistance was tested against the panel of 76 compounds in the presence or absence of the inhibitor of the primary target as described above (schema in Fig. 1A). For patient-derived resistance models with gatekeeper resistance mutations in the driver oncogene (i.e, *EGFR* or *ALK*), next-generation inhibitors that overcome those mutations were used as the primary TKI in the combination screen. The results from the initial screening were analyzed to determine the specific thresholds of GI50 and AUC changes most likely to yield a strong effect on viability and maximize the potential for in vivo efficacy (see Materials and Methods and databases S2 to S4). The process of screening and evaluating hits is demonstrated for the cell line MGH170-1BB in Fig. 1, A to C. These cells were derived from a patient with an *EGFR* mutant lung cancer who had become resistant to multiple lines of EGFR TKIs (table S2 and Fig. 1B). The screen clearly identified MET inhibitors as hits (Fig. 1C), and MET inhibitors effectively resensitized these resistant cells to EGFR inhibition (Fig. 1D, top, screen format; bottom, dose response to gefitinib as a single agent or in the presence of a fixed concentration of the MET inhibitor crizotinib). The combination of EGFR and MET inhibitors was synergistic across a range of concentrations tested, with an average of 25% lower viability than predicted by the Bliss independence model for the nine concentrations tested (see table S8 for synergy calculations). Indeed, EGFR and MET inhibitor combination therapy was effective in eliminating resistant cells (Fig. 1E). Subsequent assessment of a paraffin-embedded biopsy from this patient's cancer demonstrated clear evidence of *MET* amplification (Fig. 1G), and quantitative polymerase chain reaction (PCR) performed on the corresponding MGH170-BB cell line confirmed *MET* amplification (Fig. 1H). Thus, the unbiased pharmacologic interrogation of the cells derived from the patient specimen

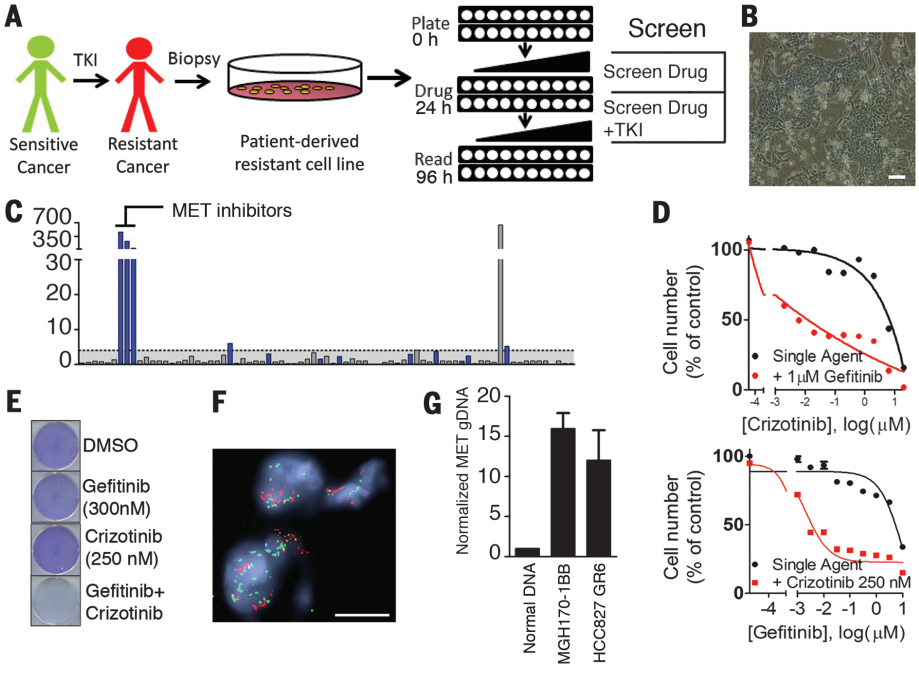

Fig. 1. Screen schematic and proof of concept in a patient-derived cell line. (**A**) Schematic of the screen workflow. Cell line models of acquired resistance were obtained directly from biopsies of patients after the development of acquired resistance to either EGFR inhibitor or ALK inhibitor in the clinic. Screen drugs were tested as a single agent and in the presence of a single fixed concentration of the primary TKI across 10 concentrations encompassing a 10,000-fold dilution range. After 72 hours, cell viability was determined with CellTiter-Glo. (**B**) Phase-contrast microscopy of cell line MGH170-1BB, derived from an *EGFR* mutant lung cancer metastatic lesion with acquired resistance to EGFR inhibitors. Scale bar, 100 μm. (**C**) Representation of screen data for the MGH170-1BB cell line. The *y* axis represents the fold-change GI50 that resulted with the addition of gefitinib (GI50 single agent/GI50 combination). Each bar is the result for an individual drug. The bars are color-coded blue when the percentage of decrease in AUC from single agent to combination was greater than 10%. Drugs were defined as "hits" when the GI50 shift was > 4 and the AUC change > 10% (see Materials and Methods). (**D**) (Top) The MET inhibitor crizotinib was more potent in combination with 1 μM gefitinib (in red) than as a single agent (in black). (Bottom) Crizotinib (1 μM) resensitizes the MGH170-1BB cells to gefitinib. Error bars, mean ± SEM. (**E**) Long-term proliferation assay of MGH170-1BB cells that had been exposed to the indicated drug for 7 days. Cells were stained using crystal violet. (**F**) Fluorescence in situ hybridization analysis of a biopsy sample from a metastatic bone lesion obtained after the patient had progressed while on treatment with erlotinib. Scale bar, 10 μm. The *MET* gene is represented in red and the *EGFR* gene in green. (**G**) Quantitative PCR analysis demonstrating overexpression of MET in MGH170-1BB in comparison with normal DNA. DNA from HCC827 GR6, which has *MET* amplification (*13*), is presented as a reference. Error bars, mean ± SEM. This experiment was repeated three times.

unequivocally indicated the combination treatment supported by genetic analyses of the patient specimen.

In some instances, pharmacologic interrogation permitted evaluation of the functional relevance of uncharacterized genetic variants. For example, a previously undescribed *FGFR3* variant was identified as a key contributor to resistance in the MGH156-1A cell line derived from a patient with acquired resistance to EGFR TKIs (fig. S4A and table S6). The screen and subsequent follow-up studies clearly indicated that fibroblast growth factor receptor (FGFR) inhibitors resensitized these cells to EGFR inhibitors. The combination also suppressed key signaling events known to regulate proliferation and survival (fig. S4, B to E). Genetic analyses of both the cell line and corresponding biopsy revealed an FGFR3 mutation, Y649C, located in the tyrosine kinase domain (table S6). Although this *FGFR3* mutation has not been observed previously (www.cbioportal.org/public-portal), it is adjacent to a recurring activating mutation in the kinase domain. Thus, in this model, combining genetic analysis of tumor material and pharmacologic evaluation of cells from the resistant tumor allowed for the identification of actionable therapeutic strategies. Furthermore, this finding demonstrates that FGFR activation is a bona fide mechanism of acquired resistance to EGFR inhibition in this patient.

Among the 60 models screened, 201 hits were identified, for a mean of 3.4 hits per cell line (range 0 to 12). At least one hit was identified in 50 of 60 cell lines (fig. S5 and Fig. 2A). Drugs known to have overlapping specificity were found to have overlapping activity across cell lines, demonstrating robustness of the data set (see, for example, aurora kinase, SRC, and MET inhibitors in Fig. 2, A and B, and fig. S5). Notably, EGFR inhibitors tended to be hits in both ALK- and MET-driven resistant lines, consistent with previously published reports (*7*, *17*). Because reactivation of the PI3K pathway via activating *PIK3CA* mutations and bypass receptor tyrosine kinases (RTKs) has commonly been observed in cancers with acquired resistance (*18*), it was not surprising that PI3K inhibitors were hits in a subset of resistant cell lines. Importantly, genetic analyses of the cell lines were insufficient to inform which cancers would be sensitive to this combination. Notably, PI3K inhibitors were not sufficient to resensitize to the original TKI in the majority of models tested (Fig. 2A and fig. S5). Other unanticipated drug combinations were identified. In particular, aurora kinase inhibitors were active in combination with EGFR inhibition in a number of *EGFR*-mutant cell lines. Similarly, the Polo-like kinase (PLK) inhibitor (BI2536) was a hit in five EGFR-driven lines. The complete hit profile of each resistant cell line is presented in fig. S6. In the in vitro models of acquired resistance (which have a paired sensitive, "parental" cell line from which the resistant cells were derived), we also sought to determine whether resistant models had developed increased sensitivity to any single-agent treatments compared with the parental cell lines (fig. S7). This analysis revealed that, in the vast majority of cases, resistant models did not acquire sensitivity to single-agent therapies, further supporting the notion of developing combination therapies (fig. S7).

Identification of mechanisms of resistance and combination therapies for *ALK*-positive lung cancers

Assessment of the patient-derived *ALK*-positive models identified previously undescribed mechanisms of resistance. The MGH034-2A cell line was derived from a biopsy of a patient harboring an *ALK*-positive cancer that had become resistant to ceritinib (LDK378), a second-generation ALK inhibitor that was recently approved by the FDA (*19*, *20*) (Fig. 3A). The MAPK kinase (MEK) inhibitor, AZD6244, was a potent hit in combination with ceritinib [Fig. 3, B and C, left panel; synergistic effect with on average 45% less viability than predicted by Bliss (table S8)]. Furthermore, AZD6244 treatment also led to marked resensitization to ceritinib in MGH034-2A (Fig. 3C, right panel). To our knowledge, there have been no previous reports demonstrating that MEK inhibitors resensitize resistant *ALK*-positive cancer cells to an ALK inhibitor. Furthermore, MEK inhibitor sensitization was not observed in any of the other *ALK*-positive patient-derived or laboratory-derived models examined in this study (fig. S8A), illustrating the potential for the present approach to identify patient-specific efficacious combinations. Long-term viability assays revealed that the combination had a potent effect on cell viability, with a marked net decrease in cell number compared to the cell number before drug treatment (Fig. 3D). Accordingly, the combination was required to inhibit PI3K, MAPK, and mammalian target of rapamycin complex (mTORC) activity, as well as to up-regulate BIM (Bcl-2 interacting mediator of cell death) and promote substantial apoptosis (*14*) (Fig. 3E and fig. S8B). In vivo, neither single agent was effective, but the combination resulted in robust tumor regression (Fig. 3F). Importantly, next-generation sequencing (NGS) analysis of the cell line revealed a MAP2K1 K57N mutation (table S7), which has previously been reported as a MEK-activating event in lung adenocarcinoma (*21*), although neither in conjunction with an activating RTK mutation nor in the setting of acquired resistance to any TKI. Notably, this cell line also harbored a JAK3 V722I variant, an activated allele of JAK3 (*22*). Despite this, the JAK3 specific inhibitor tofacitinib was not a screen hit (fig. S5) and, furthermore, did not resensitize MGH034-2A cells or other *ALK*-positive mutant cell lines to ALK inhibition (fig. S9A). Indeed, these cells did not express appreciable levels of JAK3 (fig. S9, B and C). This patient subsequently died, and NGS analysis of 10 resistant lesions acquired at autopsy demonstrated that the MAP2K1 K57N mutation was present in 7 of the 11 lesions (of

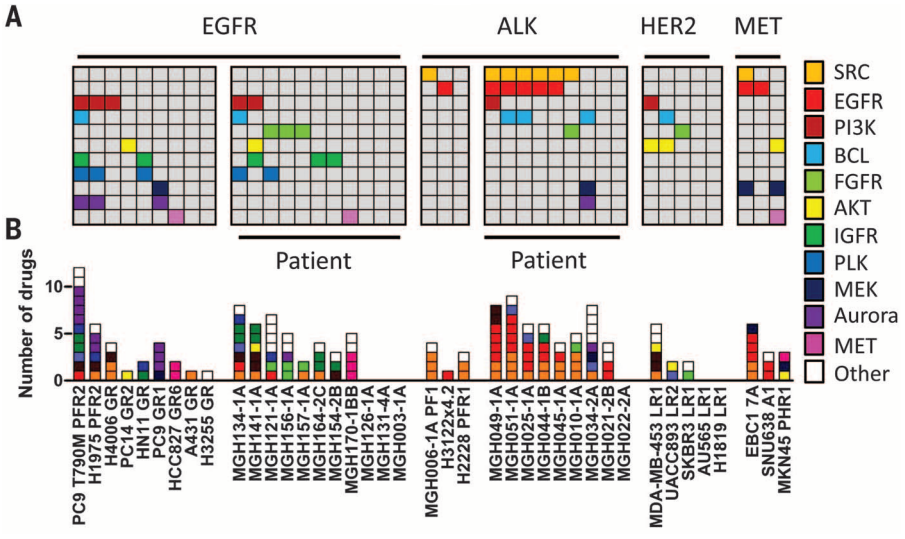

Fig. 2. Representation of selected screen hits in independent resistant models. (**A**) The patterns of hits across cell lines harboring the indicated oncogene are shown. Each column represents a cell line, and each row represents a target inhibited by the following drugs: Afatinib (EGFR), AZD0530 (SRC), BYL719 (PI3Kalpha), ABT-263 [B cell lymphoma (BCL)–2 family], Dovitinib or BGJ-398 (FGFR), MK2206 (AKT), OSI906 (IGFR), BI2536 (PLK), AZD6244 (MEK), AZD1152-HQPA (Aurora kinase B), and MGCD265 (MET). Each drug is color-coded as indicated. (**B**) The number and profile of all hit drugs for each model. Each box represents a single drug, and the drugs are color-coded by target. The white boxes indicate a hit that corresponds to a drug that is not among the targets listed. For resistant lines derived from a single parental line, only one representative model is presented except in the case of PC9, for which PC9 GR1 and PC9 GR2 are both presented due to the presence of a T790M mutation in PC9 GR2 only.

note, a PIK3CA mutation was identified in one of the other lesions) (Fig. 3H). Importantly, the MAP2K1 K57N mutation was found in the lesions that were rapidly progressing and led to respiratory failure, which caused the patient's death. The autopsy revealed that the JAK3 mutation was a germline variant, supporting the functional data that JAK3 activity was not driving resistance. These results suggest that a combination of MEK and ALK inhibitors may have provided a therapeutic benefit to this patient had these drugs been administered after the cancer had acquired resistance to ceritinib. Importantly, these results also suggest that functional assessment adds information to that provided by genetic analysis alone. Genetic profiling of the tumor alone, as is often performed in the clinic, would not have discriminated between targeting the MAP2K1 K57N mutation and the less consequential JAK3 V722I mutation.

SRC signaling mediates acquired resistance in *ALK*-positive NSCLC

Multiple SRC family kinase inhibitors were consistently effective across several patient-derived *ALK*-positive resistant NSCLC models (Fig. 2). In particular, AZD0530 (saracatinib) was a hit in six of nine patient-derived ALK lines tested (Fig. 2A). Models in which AZD0530 was a screen hit had unremarkable sensitivity to single-agent AZD0530, indicating that, as in other cases, these cell lines have not switched to an entirely different dependency. On the other hand, these resistant *ALK*-positive cell lines were highly sensitive to AZD0530 in the presence of ALK inhibitors (Fig. 4A). Drug synergism between AZD0530 and ALK inhibitors was also observed (average of 20% less viability than expected across all concentrations for five models retested in triplicate, with maximum differences ranging from 18 to 45% over Bliss (table S8). Two other drugs (dasatinib and KIN001-113) that potently inhibit Src family kinases (SFKs) (*23*, *24*) were often hits in models in which AZD0530 was a hit (Fig. 2B and fig. S5). However, due to the more favorable specificity profile of AZD0530 (*25*), we used this drug in our subsequent studies. Each model in which AZD0530 was a hit (as indicated by arrows in Fig. 4A) was significantly sensitized to ALK inhibition by AZD0530 (Fig. 4B). Notably, other *ALK*-positive models also demonstrated shifts in sensitivity, with AZD0530 pointing to the possibility of broad involvement of SRC kinases in ALK inhibitor response. Interestingly, AZD0530 was not a hit in any of the mutant *EGFR*- or *HER2*-amplified cancers and in only one of nine *MET*-amplified cancers (fig. S5).

We next aimed to determine the relevant target of AZD0530. Overexpression of the kinase-dead SRC K295R (*26*), as well as knockdown of SRC alone with either of two short-hairpin RNAs (shRNAs), effectively recapitulated the effect of AZD0530, demonstrating that among AZD0530 targets, including multiple SFKs, SRC inhibition is sufficient to resensitize cells to ALK inhibition (Fig. 4C). We observed that multiple *ALK*-positive models were sensitive to both SRC and EGFR inhibitors when combined with an ALK inhibitor. However, the activity of AZD0530 does not appear to be driven by EGFR inhibition directly or indirectly, because AZD0530 did not inhibit EGFR activation in the *ALK*-positive MGH025-1A cells, which were sensitized by AZD0530 (fig. S10A). Furthermore, some cell lines, such as MGH010-1A, were sensitized by AZD0530 but not EGFR inhibitors (Fig. 2A and fig. S10B). We next examined the effect of combined ALK and SRC inhibition on three resistant *ALK*-positive models derived from patient biopsies: MGH010-1A and MGH025-A (resistant to crizotinib, no *ALK* resistance mutations) and MGH049-1A [resistant to ceritinib, no *ALK* resistance mutations (*27*)]. In all three models, cells grew at 6 days when treated with either drug as a single agent, but combination treatment resulted in loss of cell viability compared with pretreatment cell number (Fig. 4D) and robust apoptotic cell death (S11A). Consistent with these results, the ALK inhibitor failed to fully inhibit downstream signaling (AKT, MAPK, or S6K) except in the presence of AZD0530 in each of these resistance models (Fig. 5A and fig. S11B).

In each of the patient-derived *ALK* models in which AZD0530 was effective (including MGH034-2A, which narrowly failed to meet our threshold for hit call for AZD0530), ALK inhibition resulted in robust up-regulation of SRC activity

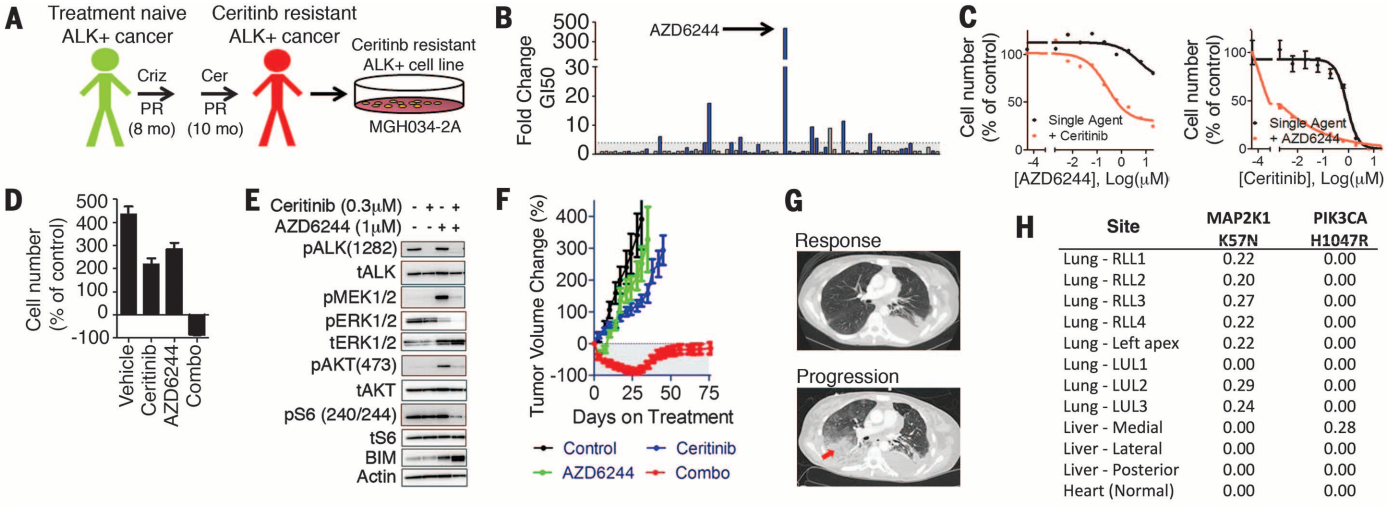

H

Site	MAP2K1 K57N	PIK3CA H1047R
Lung - RLL1	0.22	0.00
Lung - RLL2	0.20	0.00
Lung - RLL3	0.27	0.00
Lung - RLL4	0.22	0.00
Lung - Left apex	0.22	0.00
Lung - LUL1	0.00	0.00
Lung - LUL2	0.29	0.00
Lung - LUL3	0.24	0.00
Liver - Medial	0.00	0.28
Liver - Lateral	0.00	0.00
Liver - Posterior	0.00	0.00
Heart (Normal)	0.00	0.00

Fig. 3. MEK activation is a mechanism of resistance to ceritinib. (**A**) Schematic of the derivation of model MGH034-2A. (**B**) Representation of screen data for the MGH034-2A cell line. The *y* axis represents the fold-change GI50 that resulted with addition of ceritinib (0.3 μM) (GI50 single agent/GI50 combination). The bars are color-coded blue when the percentage of decrease in AUC from single agent to combination was greater than 10%. (**C**) (Left) Primary screen data of the effect of ceritinib (0.3 μM) on AZD6244 effect in MGH034-2A. (Right) A dose-response curve to ceritinib is shown in the presence and absence of a fixed concentration of the MEK inhibitor AZD6244 (1 μM). (**D**) Viability assay of MGH034-2A cells demonstrating the change in cell number after 6 days of treatment with vehicle, ceritinib (300 nM), AZD6244 (1 μM), or the combination of both drugs in comparison with the number of cells at the initiation of drug exposure. (**E**) Western blot analysis of MGH034-2A. Cells were treated with vehicle, ceritinib (0.3 μM), AZD6244 (1 μM), or the combination of both drugs for 24 hours. Lysates were analyzed with antibodies to the indicated proteins. (**F**) Subcutaneous xenografts of MGH034-2A grown in mice were used to determine in vivo efficacy by measuring change in tumor volume when treated as indicated. *n* = 6 mice per group. (**G**) Axial computed tomography images of the chest demonstrate the patient's disease burden after responding to ceritinib (5.5 weeks on treatment) and at the time of progression on ceritinib (after 9.5 months on treatment). The site of progression in the right lower lobe is indicated by an arrow. (**H**) Table of allele frequencies for MAP2K1 and PIK3CA mutations discovered at autopsy in the patient.

as measured by the phosphorylation of the SRC substrate Paxillin (Fig. 5B). Thus, ALK inhibition may lead to up-regulation of SRC signaling, perhaps by release of a negative regulatory signal normally coordinating ALK and SRC activities. In contrast, we did not consistently observe an increase in SRC activity as measured by p-Paxillin in EGFR mutant cancers after EGFR inhibitor treatment (fig. S11C), consistent with the absence of efficacy noted with AZD0530 in EGFR mutant cancer. Furthermore, in the *ALK*-positive models, SRC signaling was also up-regulated by inhibition of signaling pathways downstream of ALK. Although the downstream pathways regulated by ALK in individual models vary, the pathway regulated by ALK tended to be the one suppressing SRC signaling. For example, when ALK inhibition primarily affected PI3K signaling but not MEK activity, PI3K inhibition up-regulated SRC signaling (fig. S12A). Moreover, when ALK inhibition suppressed both MAPK and PI3K signaling, SRC signaling was robustly up-regulated by either PI3K or MAPK signaling (fig. S12B). Overall, these results are compatible with a model in which ALK activity suppresses SRC activity broadly in the setting of *ALK*-positive cancers.

To further characterize the effect of ALK inhibition on these models, we performed gene expression analysis on each of the *ALK*-positive patient-derived models in the presence or absence of an ALK inhibitor for 24 hours. The gene ontologies most enriched within genes whose expression was induced by ALK inhibition were extracellular matrix and basal membrane (Benjamini-Hochberg corrected P values 1.75×10^{-4} and 2.31×10^{-4}) (Fig. 5C and databases S6 to S8). Because SRC is known to be a focal point of integrin-mediated signaling and the transduction of extracellular signals, these results further support the finding that SRC activity is increased upon inhibition of ALK signaling in *ALK*-positive lung cancers.

Finally, we tested the efficacy of the combination of ALK TKIs and AZD0530 in vivo using mouse xenograft models. In MGH025-1A (derived from an *ALK*-positive patient who had become resistant to crizotinib), treatment with single-agent crizotinib resulted in tumor progression after 34 days. However, combining AZD0530 and crizotinib resulted in a sustained, profound response for more than 60 days (Fig. 5D). Notably, when AZD0530 was added to the treatment of the xenografts that had progressed on crizotinib, the tumors regressed (fig. S13A). To assess the specificity of AZD0530 for resistant models that demonstrated synergy in the screen, we tested it in the HCC827 GR6 line, which harbors a MET bypass track and was not a hit for AZD0530. In this model, the combination of AZD0530 with gefitinib was ineffective in comparison to gefitinib plus crizotinib (which is a potent MET inhibitor) (fig. S13B). Thus, the effect of AZD0530 appears particular to the models in which combination efficacy was found in the screen.

Because we observed impressive activity of the SFK inhibitors in a large proportion of patient-derived *ALK*-positive resistant models, we also determined whether the combination of ALK inhibitor with AZD0530 might delay the emergence of acquired resistance in a relatively sensitive model. We examined cell line MGH045-1A, a model established from a patient tumor resistant to crizotinib due to the acquisition of a mutation in the ALK kinase domain gatekeeper residue (L1196M) (table S2) (*27*). Ceritinib, which can overcome the L1196M mutation, was used as the primary TKI in the screen of this cell line, and AZD0530 was a hit (Fig. 2A). The cell line is relatively sensitive to the next-generation ALK inhibitor ceritinib, which can effectively suppress L1196M (*27*). Over 6 days of treatment in vitro, single-agent ceritinib effectively inhibited growth, but the combination of ceritinib and AZD0530 resulted in near-complete obliteration of cell viability (Fig. 4D). Accordingly, both ALK inhibition and AZD0530 were required to completely suppress key downstream signaling events (fig. S13C). In vivo, single-agent ceritinib slowed tumor growth as previously described (*27*), but the combination resulted in a more sustained response (fig. S13D). This reinforces the notion that initial treatment combining a SRC and an ALK inhibitor could help induce a more sustained response in patients with *ALK*-positive lung cancer.

Analysis of the discovered mutations identified by the 1000-gene NGS panel in the *ALK*-positive

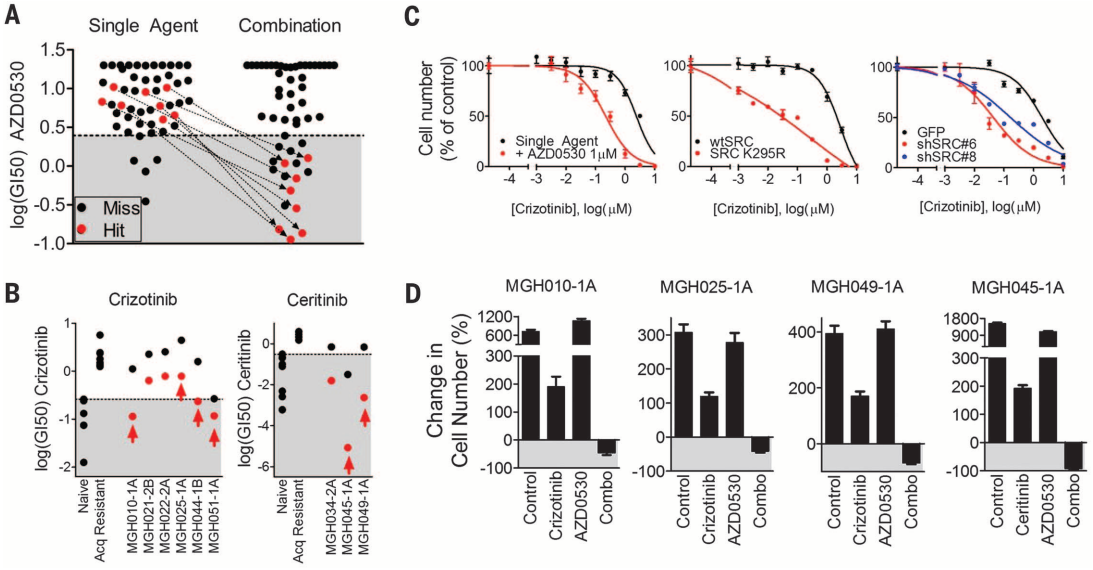

Fig. 4. SRC inhibition restores sensitivity to ALK inhibitor in multiple models. (**A**) Representation of the GI50 of AZD0530 in each screened model as a single agent or in combination with the primary TKI. Models that were hits are color-coded red. The GI50s of cell lines in which AZD0530 scored as hits are connected by an arrow. The shaded area represents the GI50 values among the top 10% sensitive models for single-agent values among all lines screened. (**B**) GI50 of each *ALK*-positive patient-derived model of acquired resistance to either crizotinib or ceritinib. Control cell line models of sensitivity (MGH006-1A, H3122, SU-DHL-1, KARPAS299, and NB-1) and acquired resistance (MGH006-1A PFR1, MGH006-1A PFR2, H2228 PFR1, H3122 PFR1, H3122 PFR3, and H3122 x4.2) to crizotinib are presented as standards for comparison. Models of sensitivity (H3122, H2228, MGH051-1B, H3122 PFR2, MGH021-2cl4, MGH006-1A, MGH026-1A, and MGH039-1A) and acquired resistance (MGH021-5, H3122 LDKR1, H3122 LDKR2, H3122 LDKR2, and H3122 LDRK4) to ceritinib are presented as standards for comparison. The GI50 of each model is presented as a single agent (black) and in combination with AZD0530 (1 μM) (red). The mean GI50 of the three experiments is presented. Arrows indicate hits identified by the screen. (**C**) Dose-response curves to crizotinib in model MGH010-1A (crizotinib resistant) are presented. (Left) The dose-response of single-agent crizotinib (black) in the absence or presence of AZD0530 (1 μM) (red). (Middle) The effect of crizotinib in cells with lentiviral overexpression of either wild-type SRC (black) or kinase-dead SRC (K295R, red). (Right) The effect of lentiviral expression of green fluorescent protein (GFP) (black) or either of two SRC-targeted shRNAs (blue and red). (**D**) Six-day viability assay of four ALK lines: MGH010-1A, MGH025-1A, MGH049-1A, and MGH045-1A. Each panel presents the percentage of change in cell number after treatment with vehicle, ALK inhibitor (crizotinib 1 μM or ceritinib 300 nM), AZD0530 (1 μM), or the combination compared with cell number at the initiation of treatment.

models failed to identify mutations in SRC family kinases and other known regulators of SRC activity (table S7). Thus, the pharmacologic approach identified a drug combination that would not have readily been predicted by DNA sequencing alone.

Discussion

In summary, we have developed cell culture models of acquired resistance to EGFR and ALK inhibition derived directly from patient specimens to rapidly identify combinations that can overcome resistance. These initial studies demonstrated success in developing NSCLC models in 50% of collected specimens. However, we believe that success rates could be further improved by using biopsies acquired specifically for cell line generation. In this study, the biopsies were prioritized for standard pathological analysis, and cell lines were generated from any remaining tissue. As a result, the quality of the specimens was less than ideal. Indeed, in the majority (24 of 39) of the "failures," the samples we analyzed contained fewer than 20% cancer cells. Despite these obstacles, cell line models were successfully developed in about half of the cases. Thus, if biopsies were isolated primarily for this purpose, we believe that this methodology could potentially be explored as a diagnostic approach to guide treatment decisions. We also anticipate that this approach will be generalizable to other solid and liquid tumor malignancies.

The robustness of the approach presented here is demonstrated by the success rate of in vivo studies. All five tested models [MGH034-2A (Fig. 3), MGH045-1A (fig. S13), MGH025-1A (Fig. 5D), PC9 PFR2 (fig. S14), and PC9 GR1 (fig. S15)] demonstrated substantial regression in vivo with the discovered active combination. Importantly, this functional assessment of patient-derived samples can provide insights not provided by genetic analysis. For example, the effect of SRC inhibition in resistant *ALK*-positive cancers is not readily predicted by genetic analyses because no mutation was identified in SFKs or their regulators. In addition, our results illustrate how functional assessment of patient-derived cells can complement genetic profiling. For example, FGFR inhibitors were effective in a model with a previously uncharacterized *FGFR3* mutation (fig. S4). In the absence of functional data, the biological consequence of the mutation would have been uncertain.

By interrogating patient-derived models of resistance with this pharmacologic platform, we have discovered several previously undescribed combinations in *EGFR* mutant and *ALK*-positive lung cancers that were validated in follow-up studies and in vivo. We speculate that a similar approach could be explored in the future as a diagnostic test to identify therapeutic strategies for individual patients (under the auspices of an IRB-approved protocol). In the current study, we screened the cells after they became fully established cell lines, which often took 2 to 6 months, a time frame that would make this approach less than ideal as a routine diagnostic test. Nevertheless, the robustness of the results from the current program lays the groundwork for performing screens on viable cells obtained within weeks of a biopsy using newer technologies that would permit screening of the cancer cells while still in the presence of the stroma present in the biopsy. Indeed, it is possible that such functional screens performed on cells derived from a biopsy of a particular patient's resistant cancer might inform the choice of experimental therapies that are most likely to be effective in that patient, advancing toward a future of truly personalized cancer therapy.

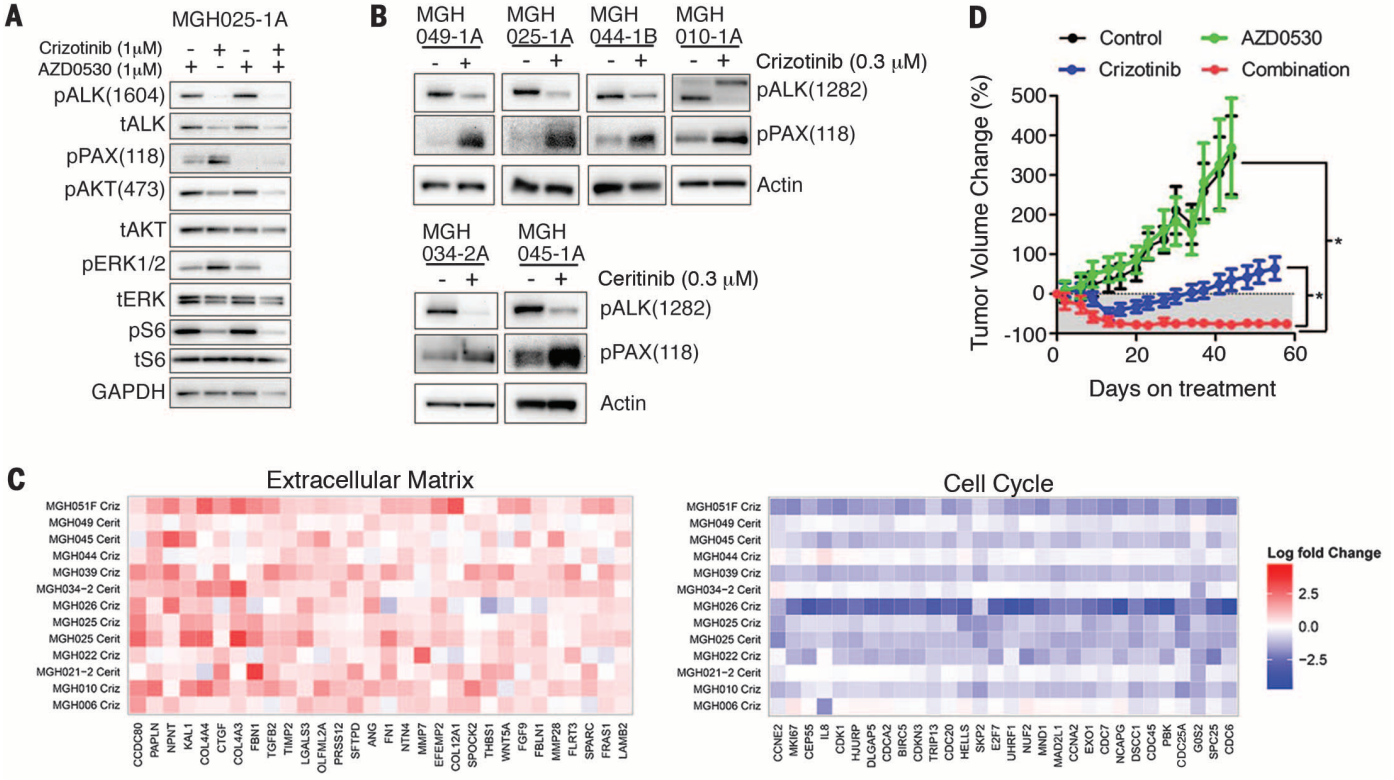

Fig. 5. ALK inhibition and SRC signaling. (**A**) Western blot analysis of MGH025-1A. Cells were treated with vehicle, crizotinib (1 μM), AZD0530 (1 μM), or the combination of both drugs for 24 hours. Lysates were analyzed with antibodies to the indicated proteins. (**B**) Western blot analysis of patient-derived resistant *ALK* models treated for 24 hours with crizotinib (300 nM) or ceritinib (300 nM). Lysates were prepared and blotted with the indicated antibodies. (**C**) Fold-change in gene expression (Log2) upon treatment with the indicated ALK inhibitor for 24 hours. (Left) Up-regulated genes annotated with the gene ontology (GO) term "extracellular matrix." (Right) Down-regulated genes annotated with the GO term "cell cycle" (top 30 genes only). (**D**) MGH025-1A subcutaneous xenografts grown in mice were treated as indicated: vehicle (n = 4 mice), crizotinib 25 mg per kg of weight (mg/kg) daily (n = 6 mice), AZD0530 50 mg/kg daily (n = 5 mice), or the combination of both drugs (n = 6 mice). Error bars, mean ± SEM. *P < 0.0001 by Dunn's multiple comparison test.

REFERENCES AND NOTES

1. A. Inoue *et al.*, *J. Clin. Oncol.* **24**, 3340–3346 (2006).
2. E. L. Kwak *et al.*, *N. Engl. J. Med.* **363**, 1693–1703 (2010).
3. R. Rosell *et al.*, *Lancet Oncol.* **13**, 239–246 (2012).
4. L. V. Sequist *et al.*, *J. Clin. Oncol.* **26**, 2442–2449 (2008).
5. A. T. Shaw *et al.*, *Lancet Oncol.* **12**, 1004–1012 (2011).
6. C. R. Chong, P. A. Jänne, *Nat. Med.* **19**, 1389–1400 (2013).
7. R. Katayama *et al.*, *Sci. Transl. Med.* **4**, 120ra17 (2012).
8. N. Yamaguchi *et al.*, *Lung Cancer* **83**, 37–43 (2014).
9. J. Tanizaki *et al.*, *Clin. Cancer Res.* **18**, 6219–6226 (2012).
10. M. J. Niederst, J. A. Engelman, *Sci. Signal.* **6**, re6 (2013).
11. X. Liu *et al.*, *Am. J. Pathol.* **180**, 599–607 (2012).
12. J. A. Engelman *et al.*, *Nat. Med.* **14**, 1351–1356 (2008).
13. J. A. Engelman *et al.*, *Science* **316**, 1039–1043 (2007).
14. A. C. Faber *et al.*, *Proc. Natl. Acad. Sci. U.S.A.* **106**, 19503–19508 (2009).
15. M. L. Sos *et al.*, *Proc. Natl. Acad. Sci. U.S.A.* **106**, 18351–18356 (2009).
16. M. Guix *et al.*, *J. Clin. Invest.* **118**, 2609–2619 (2008).
17. J. Qi *et al.*, *Cancer Res.* **71**, 1081–1091 (2011).
18. L. V. Sequist *et al.*, *Sci. Transl. Med.* **3**, 75ra26 (2011).
19. T. H. Marsilje *et al.*, *J. Med. Chem.* **56**, 5675–5690 (2013).
20. A. T. Shaw *et al.*, *N. Engl. J. Med.* **370**, 1189–1197 (2014).
21. J. L. Marks *et al.*, *Cancer Res.* **68**, 5524–5528 (2008).
22. D. K. Walters *et al.*, *Cancer Cell* **10**, 65–75 (2006).
23. M. W. Karaman *et al.*, *Nat. Biotechnol.* **26**, 127–132 (2008).
24. U. McDermott, R. V. Pusapati, J. G. Christensen, N. S. Gray, J. Settleman, *Cancer Res.* **70**, 1625–1634 (2010).
25. L. F. Hennequin *et al.*, *J. Med. Chem.* **49**, 6465–6488 (2006).
26. S. Bagrodia, I. Chackalaparampil, T. E. Kmiecik, D. Shalloway, *Nature* **349**, 172–175 (1991).
27. L. Friboulet *et al.*, *Cancer Discov.* **4**, 662–673 (2014).

ACKNOWLEDGMENTS

We thank L. H. Park for direction, redirection, and support; S. R. Vora for continual critical discussion and support; W. Michaud for providing feeder cells and training for the development of patient-derived cell lines; and N. Gray for providing several kinase inhibitors. This study was funded by support from the NIH R01CA137008 (J.A.E.), R01CA164273 (A.T.S. and J.A.E.), 1U54HG006097-01 (C.H.B.), the Wellcome Trust (086357 and 102696, C.H.B.), the National Cancer Institute Lung SPORE P50CA090578 (A.S.C., A.J.I., and J.A.E.), the Department of Defense (L.V.S. and J.A.E.), Conquer Cancer Foundation Young Investigator Award (A.S.C.), Uniting Against Lung Cancer (A.S.C. and A.T.S.), Free to Breathe (A.S.C.), Lungevity (L.V.S. and J.A.E.), National Foundation for Cancer Research (A.T.S.), and Be a Piece of the Solution.
J.A.E. is a paid consultant for Novartis, Sanofi-Aventis, AstraZeneca, Chugai, Amgen, Genentech, GSK, Merck, and Pfizer, and he holds equity in Gatekeeper Pharmaceuticals, which has a potential equity interest in T790M inhibitors. J.A.E. also receives research support from Novartis. J.F.G. is a paid consultant for Boehringer Ingelheim. A.T.S. is a paid consultant for Pfizer, Novartis, Ariad, Chugai, Genentech, Roche, and Ignyta. A.J.I. is a Senior Advisory Board member and holds equity in Enzymatics Inc. For gene expression analyses, the raw data are deposited in ArrayExpress (accession number is E-MTAB-783). The normalized data are available at www.cancerrxgene.org/downloads.

SUPPLEMENTARY MATERIALS

www.sciencemag.org/content/346/6216/1480/suppl/DC1
Materials and Methods
Figs. S1 to S16
Tables S1 to S8
Databases S1 to S8
References (*28*–*34*)

14 April 2014; accepted 21 October 2014
Published online 13 November 2014;
10.1126/science.1254721

HUMORAL IMMUNITY

MAVS, cGAS, and endogenous retroviruses in T-independent B cell responses

Ming Zeng,[1] Zeping Hu,[2]* Xiaolei Shi,[2]* Xiaohong Li,[1]* Xiaoming Zhan,[1]* Xiao-Dong Li,[1,4] Jianhui Wang,[1,4] Jin Huk Choi,[1] Kuan-wen Wang,[1] Tiana Purrington,[1] Miao Tang,[1] Maggy Fina,[1] Ralph J. DeBerardinis,[2] Eva Marie Y. Moresco,[1] Gabriel Pedersen,[3] Gerald M. McInerney,[3] Gunilla B. Karlsson Hedestam,[3] Zhijian J. Chen,[1,4] Bruce Beutler[1]†

Multivalent molecules with repetitive structures including bacterial capsular polysaccharides and viral capsids elicit antibody responses through B cell receptor (BCR) crosslinking in the absence of T cell help. We report that immunization with these T cell–independent type 2 (TI-2) antigens causes up-regulation of endogenous retrovirus (ERV) RNAs in antigen-specific mouse B cells. These RNAs are detected via a mitochondrial antiviral signaling protein (MAVS)–dependent RNA sensing pathway or reverse-transcribed and detected via the cGAS-cGAMP-STING pathway, triggering a second, sustained wave of signaling that promotes specific immunoglobulin M production. Deficiency of both MAVS and cGAS, or treatment of MAVS-deficient mice with reverse transcriptase inhibitors, dramatically inhibits TI-2 antibody responses. These findings suggest that ERV and two innate sensing pathways that detect them are integral components of the TI-2 B cell signaling apparatus.

Specific antibody production is a hallmark of the B cell response to antigens. T cell–dependent (TD) antibody responses typically elicited by protein antigens require follicular helper T cells for full B cell activation, proliferation, and antibody production. In contrast, T cell–independent (TI) antigens stimulate antibody production in the absence of major histocompatibility complex (MHC) class II–restricted T cell help. TI antigens include the TI type 1 (TI-1) antigens, which engage Toll-like receptors (TLRs) in addition to the B cell receptor (BCR), and TI type 2 (TI-2) antigens, which engage the BCR in a manner that induces extensive crosslinking, leading to BCR activation and immunoglobulin M (IgM) production. TI-2 antigens are large multivalent molecules with highly repetitive structures, such as bacterial capsular polysaccharides and viral capsids (*1*).

B cell–intrinsic cytosolic DNA and RNA sensing in the TI-2 antibody response

We tested the requirement for innate immune sensing pathways in the antibody response to the model TI-2 antigen 4-hydroxy-3-nitrophenylacetyl-Ficoll (NP-Ficoll) by monitoring anti-NP IgM in the serum of mice after immunization (*2*). C57BL/6J mice mounted a robust NP-specific IgM response by day 4.5 after immunization, which peaked around day 14.5 after immunization (Fig. 1A and fig. S1). Similarly, mice that could not signal via NLRP3, TLR3, TLR7, TLR9, TLR2, TLR4, CD36, MyD88, TICAM1, or IRAK4, all nucleic acid–sensing TLRs (*Unc93b1*$^{3d/3d}$), or all TLRs (*Ticam1*$^{Lps2/Lps2}$; *Irak4*$^{otiose/otiose}$) produced normal levels of NP-specific IgM on day 4.5 after immunization (Fig. 1A). In contrast, *Tmem173*$^{gt/gt}$ mice and *Mb21d1*$^{-/-}$ mice, deficient in the cytosolic DNA-sensing pathway components stimulator of interferon gene (STING) and cGMP-AMP synthase (cGAS), respectively, exhibited suboptimal IgM responses to NP-Ficoll on day 4.5 and for up to 30 days after immunization (Fig. 1A and fig. S1). Mice lacking mitochondrial antiviral signaling protein (MAVS), an adaptor for the cytoplasmic RNA-sensing RIG-I–like helicases, also produced diminished amounts of NP-specific IgM (Fig. 1A and fig. S1). Antibody responses to the TI-1 antigen NP-LPS (LPS, lipopolysaccharide) (Fig. 1B), and the TD antigen β-galactosidase (β-gal) encoded by a nonreplicating recombinant Semliki Forest virus (rSFV) vector (*3*) (Fig. 1C), were normal in STING-, cGAS-, and MAVS-deficient mice.

We evaluated marginal zone (MZ) and B-1 B cell populations in STING-, cGAS-, and MAVS-deficient mice and found no deficiencies in frequencies or numbers (fig. S2 and supplementary text), except in the NP-specific populations after NP-Ficoll immunization (fig. S3). Also, NP-Ficoll capture by MZ B cells and MZ macrophages was normal in the mutant mice (fig. S4).

We performed adoptive transfer of C57BL/6J, STING-, cGAS-, or MAVS-deficient splenic and

[1]Center for the Genetics of Host Defense, University of Texas Southwestern Medical Center, 5323 Harry Hines Boulevard, Dallas, TX 75390-8502, USA. [2]Department of Pediatrics and Children's Medical Center Research Institute, and McDermott Center for Human Growth and Development, University of Texas Southwestern Medical Center, 5323 Harry Hines Boulevard, Dallas, TX 75390-8502, USA. [3]Department of Microbiology, Tumor and Cell Biology, Karolinska Institutet, Nobels väg 16, SE-171 77 Stockholm, Sweden. [4]Howard Hughes Medical Institute, Department of Molecular Biology, University of Texas Southwestern Medical Center, 5323 Harry Hines Boulevard, Dallas, TX 75390-9148, USA.
*These authors contributed equally to this work. **†Corresponding author. E-mail: Bruce.Beutler@UTSouthwestern.edu**